Photochemical and Chemical Oxidation of α-Dimine−Dithiolene Metal Complexes: Insight into the Role of the Metal Atom

T. Matthew Cocker and Robert E. Bachman*

Department of Chemistry, Box 571227, Georgetown University, Washington, D.C., 20057-1227

Received August 4, 2000

[Pd(bpy)(bdt)], **2** (bpy = 2,2′-bipyridine, bdt = 1,2-benzenedithiolate), was prepared in good yield by the reaction of $bdtNa_2$ with $[(bpy)PdCl_2]$ in DMSO. The analogous nickel complex, **1**, was prepared in a similar reaction using $MeOH/CH_2Cl_2$ and $[(bpy)NiCl_2{\cdot}dmf]_2$. Both **1** ($a$ = 7.9920(1) Å, b = 11.4385(1) Å, c = 16.1415(1) Å, β = 103.327(1)°, V = 1435.86(2) Å^3, Z = 4) and **2** (a = 8.1631(5) Å, b = 11.4379(7) Å, c = 16.2475(10) Å, β = 103.7010(10)°, V = 1473.84(12) Å^3, Z = 4) crystallize in the monoclinic space group $P2_1/c$ and are isostructural with their previously reported platinum analogue. In accord with the results observed for platinum but not nickel, photochemical oxidation of **2** in DMF provides the monosulfinate complex [Pd(bpy)($bdtO_2$)], **4**, along with a minor amount of the corresponding disulfinate [Pd(bpy)($bdtO_4$)], **5**, while chemical oxidation yields only the latter. **4** cocrystallizes with **5** in the monoclinic space group $P2_1/c$ (a = 8.026(3) Å, b = 14.600(6) Å, c = 13.371(3) Å, β = 101.80(3)°, V = 1533.8(9) Å^3, Z = 4) as does pure **5** (a = 8.5611(9) Å, b = 14.4586(15) Å, c = 13.3677(14) Å, β = 108.122(2)°, V = 1572.6(3) Å^3, Z = 4). Comparison of spectroscopic and electrochemical properties of the three complexes, [M(bpy)(bdt)], yields the following ordering for the energy of the HOMO: Pd < Ni < Pt. The observed reactivity patterns and the electronic data suggest that the "anomalous" reactivity of **1** be attributed to the greater relative flexibility of the coordination geometry for nickel(II) complexes rather than electronic differences such as the energies of the frontier orbitals.

Introduction

Over the past quarter-century dithiolene-α-diimine (**A**), dithiolato-α-diimine (**B**), and dithiolato-α-diamine (**C**) complexes of the group VIII metals have attracted the attention of numerous research groups because of their unique properties, which include solution luminescence, solvatochromism, large molecular hyperpolarizabilities, and large excited-state oxidation potentials.[1−4] In particular, much of this work has focused on

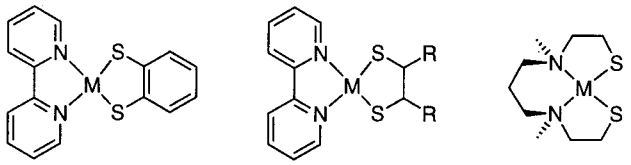

the optoelectronic properties of the platinum(II) complexes of types **A** and **B**. Additionally, interest in nickel(II)-containing complexes of type **C** has been fueled by their ability to act as models for biological systems such as CO-dehydrogenase, which contains a Ni−S moiety at the reactive center of the enzyme.[5−7] Interestingly, despite the significant structural and electronic variation among the systems that have been explored thus far, photochemical or chemical oxidation has resulted in dithiolene/dithiolato-centered rather than metal-centered oxidation.[3e,5−9]

In 1985 Srivastava and co-workers first suggested that the type **A** complexes [Pt(bpy)(tdt)] and [Pd(bpy)(tdt)] (bpy = 2,2′-bipyridine; tdt = 3,4-toluenedithiolato) both exhibited the ability to act as a photosensitizer for the formation of singlet oxygen. They attributed this ability to the unique LLCT-based excited state of these complexes;[3e] however, they were unable to fully characterize the photooxidation products of these reactions.

(1) Miller, T. R.; Dance, I. G. *J. Am. Chem. Soc.* **1973**, *95*, 6970−6979.
(2) (a) Connick, W. B.; Geiger, D.; Eisenberg, R. *Inorg. Chem.* **1999**, 3264−3265. (b) Paw, W.; Lachicotte, R. J.; Eisenberg, R. *Inorg. Chem.* **1998**, *37*, 4139−4141. (c) Cummings, S. D.; Cheng, L.-T.; Eisenberg, R. *Chem. Mater.* **1997**, *9*, 440−450. (d) Cummings, S. D.; Eisenberg, R. *J. Am. Chem. Soc.* **1996**, *118*, 1949−1960. (e) Cummings, S. D.; Eisenberg, R. *Inorg. Chem.* **1995**, *34*, 2007−2014. (f) Paw, W.; Cummings, S. D.; Mansour, M. A.; Connick, W. B.; Geiger, D. K.; Eisenberg, R. *Coord. Chem. Rev.* **1998**, *171*, 125−150 and references therein.
(3) Islam, A.; Sugihara, H.; Hara, K.; Singh, L. P.; Katoh, R.; Yanagida, M.; Takaashi, Y.; Murata, S.; Arakawa, H. *New J. Chem.* **2000**, *24*, 343−345. (b) Keefer, C. E.; Bereman, R. D.; Purrington, S. T.; Knight, B. W.; Boyle, P. D. *Inorg. Chem.* **1999**, *38*, 2294−2302. (c) Chen, C.-T.; Liao, S.-Y.; Lin, K.-J.; Chen, C.-H.; Lin, T.-Z. J. *Inorg. Chem.* **1999**, *38*, 2734−2741. (d) Vicente, R.; Ribas, J.; Cassoux, P.; Sourisseau, C. *Synth. Met.* **1986**, *15*, 79−89. (e) Puthraya, K. H.; Srivastava, T. S. *Tetrahedron* **1985**, *4*, 1579−1584. (f) Vogler, A.; Kunkley, H.; Hlavatsch, J.; Merz, A. *Inorg. Chem.* **1984**, *23*, 506−509.
(4) (a) Base, K.; Tierney, M. T.; Muller, J.; Grinstaff, M. W. *Inorg. Chem.* **1999**, *38*, 287−289. (b) Base, K.; Grinstaff, M. W. *Inorg. Chem.* **1998**, *37*, 1432−1433.
(5) (a) Grapperhaus, C. G.; Darensbourg, M. Y. *Acc. Chem. Res.* **1998**, *31*, 451−459. (b) Bellefeuille, J. A.; Grapperhaus, C. A.; Buonomo, R. M.; Reibenspies, J. H.; Darensbourg, M. Y. *Organometallics* **1998**, *17*, 4813−4821. (c) Grapperhaus, C. A.; Maguire, M. J.; Tuntulani, T.; Darensbourg, M. Y. *Inorg. Chem.* **1997**, *36*, 1860−1866. (d) Grapperhaus, C. A.; Darensbourg, M. Y.; Sumner, L. W.; Russell, D. H. *J. Am. Chem. Soc.* **1996**, *118*, 1791−1792. (e) Darensbourg, M. Y.; Tuntulani, T.; Reibenspies, J. H. *Inorg. Chem.* **1995**, *34*, 6287−6294. (f) Tuntulani, T.; Musie, G.; Reibenspies, J. H.; Darensbourg, M. Y. *Inorg. Chem.* **1995**, *34*, 6279−6286. (g) Buonomo, R. M.; Font, I.; Maguire, M. J.; Reibenspies, J. H.; Tuntulani, T.; Darensbourg, M. Y. *J. Am. Chem. Soc.* **1995**, *117*, 963−973.
(6) Maroney, M. J.; Choudhury, S. B.; Bryngelson, P. A.; Mirza, S. A.; Sherrod, M. J. *Inorg. Chem.* **1996**, *35*, 1073−1076. (b) Mirza, S. A.; Day, R. O.; Maroney, M. J. *Inorg. Chem.* **1996**, *35*, 1992−1995.
(7) Henderson, R. K.; Bouwman, E.; Spek, A. L.; Reedijk, J. *Inorg. Chem.* **1997**, *36*, 4616−4617.

10.1021/ic000884n CCC: $20.00 © 2001 American Chemical Society
Published on Web 02/23/2001

Since this initial report, the chemical and photochemical oxidation of nickel-containing complexes, principally of type **C**, has been studied extensively. Depending on the reaction conditions, a wide variety of products have been isolated—monosulfenates [RS−M−SOR], disulfenates [M−$(SOR)_2$], monosulfinates [RS−M−SO_2R], disulfinates [M−$(SO_2R)_2$], mixed sulfinate−sulfenate [ROS−M−SO_2R], and disulfonate [M−$(SO_3R)_2$].[5,7,8] The formation of the disulfonate complexes is particularly noteworthy because they involve the oxidative cleavage of the hypothetically strong metal−sulfur bonds.

More recently, attention has again shifted to the heavier members of the triad, with palladium(II) complexes of type **C** and platinum(II) complexes of type **B** being shown to undergo photoinduced oxidation in the presence of atmospheric oxygen to yield monosulfenate, disulfenate, mixed sulfinate/sulfenate, monosulfinate, and disulfenate complexes.[5,10] Additionally, Connick and Gray recently reported the complete structural and spectroscopic characterization of the photooxidation products of [Pt(bpy)(bdt)] (**3**) (bdt = 1,2-benzenedithiolato), identifying both a monosulfinate and a disulfinate complex depending on the oxidation conditions.[9] In contrast to their findings, we recently reported that the corresponding nickel complex, [Ni(bpy)(bdt)] (**1**), is readily oxidized to an octahedral disulfonate complex in a process that involves substantial ligand scrambling.[8] The widely differing behavior of these two closely related complexes naturally raises the question of the role that the metal atom plays in the oxidation process. In an attempt to address this question, we decided to study the oxidation behavior of the third member of this family, [Pd(bpy)(bdt)] (**2**). In this paper, we report an improved synthesis of **1**−**3**, the structural characterization of **1** and **2**, and the complete characterization of the photochemical and chemical oxidation products of **2**. On the basis of the data accumulated both here and in the literature, we also suggest a rationalization for the "anomalous" oxidation behavior of **1**.

Experimental Procedures

Materials. All solvents were purified prior to use by distillation unless otherwise stated and carefully ensured to be peroxide-free using standard procedures.[11] The chemicals bpy, bpy$PdCl_2$, bpy$PtCl_2$, and 30% H_2O_2 were purchased from Aldrich and used as received. $NiCl_2$-(anhydrous) was prepared by drying $NiCl_2 \cdot 6H_2O$ (Aldrich) at >230 °C for 7 days and then cooling the anhydrous material in a desiccator. The sodium salt of bdt, ($bdtNa_2$),[12] and [bpy$NiCl_2$(dmf)]$_2$[13] were prepared according to literature procedures.

Physical Measurements. ^{1}H NMR spectra were recorded on a Varian Mercury 300 NMR spectrometer in the solvents specified and referenced to TMS ($\delta = 0$ ppm). Electrochemical measurements were performed using a Cypress Systems Inc. CS-1200 potentiostat system with a gold working electrode, a platinum auxiliary electrode, and a silver wire pseudoreference electrode. The measurements were carried out at room temperature in nitrogen-saturated benzonitrile solutions containing ca. 0.06 M [(n-Bu)$_4$N][PF_6] as the supporting electrolyte. The ferrocene−ferrocenium couple (taken as zero volts) was used as an internal reference, and values are quoted relative to that couple.[14] The potentials of reversible processes were taken as their $E_{1/2}$ values, while the potentials of irreversible processes were taken to be their peak anodic currents.

Synthesis of [Ni(bpy)(bdt)], 1. $C_6H_4S_2Na_2$ (18.6 mg, 0.10 mmol) dissolved in 10 mL of MeOH was added to a solution of [bpy$NiCl_2$-(dmf)]$_2$ (35.9 mg, 0.05 mmol) in 40 mL of CH_2Cl_2, resulting in an instant color change from pale green to dark purple. The reaction mixture was stirred at room temperature for 12 h and then warmed to reflux for 1 h. After the mixture was allowed to cool, the solvents were removed by rotary evaporator and the dark-purple solid was washed with MeOH followed by ether to give **1**. Yield: 26 mg (73% based on Ni); mp = 210−212 °C. λ_{max} (MeOH): 517 nm, (MeCN) 520 nm, ($CHCl_3$) 557 nm (ϵ($CHCl_3$) = 2500 M^{-1} cm^{-1}). ^{1}H NMR (DMSO, ppm): 6.72 (m, 2H), 7.04 (m, 2H), 7.70 (m, 2H), 8.25 (t, 2H, J = 6.4 Hz), 8.49 (d, 2H, J = 5.3 Hz), 8.66 (d, 2H, J = 4.7 Hz). X-ray quality crystals were grown by slow evaporation of a DMF solution in the dark at room temperature.

Synthesis of [Pd(bpy)(bdt)], 2. An amount of 59 mg of $C_6H_4S_2$-Na_2 (0.316 mmol) was added with stirring to 105.4 mg (0.316 mmol) of bpy$PdCl_2$ dissolved in 30 mL of deoxygenated DMSO under a nitrogen atmosphere. The solution turned instantly from yellow to dark-red upon addition of the thiolate. The reaction mixture was stirred at room temperature for 18 h, then warmed to 50 °C for 1 h. After the mixture was cooled to room temperature, the solution was added to 200 mL of ice water and the resulting red suspension was cooled to 5 °C for 18 h. The dark-red precipitate was collected by filtration and then washed with MeOH followed by ether. Yield: 84 mg (66% based on Pd); mp = 240 °C. ^{1}H NMR (DMSO, ppm): 6.75 (dd, 2H, J = 5.1, 3.4 Hz), 6.99 (dd, 2H J = 5.1, 3.4 Hz), 7.80 (t, 2H, J = 6.4 Hz), 8.32 (t, 2H, J = 7.7 Hz), 8.65 (s, 2H), 8.67 (s, 2H). λ_{max} ($CHCl_3$): 510 nm (ϵ($CHCl_3$) = 2600 M^{-1} cm^{-1}). X-ray quality crystals were grown by slow evaporation of a CH_2Cl_2 solution in the dark at room temperature.

Synthesis of [Pt(bpy)(bdt)], 3. The purple complex was synthesized according to the same method as for **2**, using bpy$PtCl_2$ (21.0 mg, 0.05 mmol), $C_6H_4S_2Na_2$ (9.3 mg, 0.05 mmol), and DMSO (20 mL). Yield: 17.7 mg (72% based on Pt); mp = 340 °C (dec). λ_{max} ($CHCl_3$): 598 nm (ϵ($CHCl_3$) = 5800 M^{-1} cm^{-1}). ^{1}H NMR (DMSO, ppm): 6.80 (dd, 2H, J = 5.7, 3.0 Hz), 7.42 (dd, 2H J = 5.7, 3.0 Hz), 7.80 (t, 2H, J = 6.4 Hz), 8.41 (t, 2H, J = 8.5 Hz), 8.62 (d, 2H, J = 7.7 Hz), 9.28 (d, 2H, J = 6.4 Hz). X-ray quality crystals were grown by slow evaporation of a CH_2Cl_2 solution in the dark at room temperature. The unit cell parameters for these crystals matched those published by Connick and Gray for crystals grown from DMF.[17]

Photochemical Oxidation of 2, [Pd(bpy)(bdtO_2)], 4. A small sample of **2** was dissolved in 15 mL of oxygen-saturated DMF and left on a well-illuminated shelf for 3 months. The color of the solution slowly turned from dark red to pale yellow as the DMF evaporated, yielding a small number of X-ray quality crystals.

Chemical Oxidation of 2, [Pd(bpy)(bdtO_4)], 5. An amount of 20 mg (0.050 mmol) of **2** dissolved in DMSO was treated with an excess of H_2O_2. The dark-red solution slowly turned golden-yellow after the addition of H_2O_2. The reaction mixture was then added to 200 mL of cold H_2O and extracted with CH_2Cl_2 (3 × 100 mL). The combined organic fractions were dried over Na_2SO_4, and the solvent was removed by rotary evaporation to give **5** as a pale-yellow solid. Yield: 15 mg (60%). ^{1}H NMR (DMSO, ppm): 7.76 (dd, 2H, J = 6.0, 3.0 Hz), 7.88 (dd, 2H, J = 6.0, 3.0 Hz), 8.02 (t, 2H, J = 6.0 Hz), 8.45 (t, 2H, J = 7.7 Hz), 8.76 (d, 2H, J = 8.1 Hz), 9.13 (d, 2H, J = 4.7 Hz). The NMR solvent was added to water (50 mL), extracted with CH_2Cl_2 (3 × 25 mL), and dried over Na_2SO_4. The solvent volume was reduced to 10 mL via rotary evaporation, and the concentrated solution was filtered. X-ray quality crystals were grown by slow evaporation of the resulting pale-yellow filtrate at room temperature.

X-ray Crystallography. 1. A dark-red plate approximately 0.50 × 0.10 × 0.08 mm^3 was mounted on a glass fiber using epoxy cement. The X-ray data were collected on a Bruker-AXS SMART CCD

(8) Cocker, T. M.; Bachman, R. E. *Chem. Commun.* **1999**, 875−876.
(9) Connick, W. B.; Gray, H. B. *J. Am. Chem. Soc.* **1997**, *119*, 11620−11627.
(10) Zhang, Y.; Ley, K. D.; Schanze, K. S. *Inorg. Chem.* **1996**, *35*, 7102−7110.
(11) Perrin, D. D.; Armarego, W. L. F. *Purification of Laboratory Chemicals*, 3rd ed.; Pergamon Press: New York, 1988.
(12) Testaferri, L.; Tiecco, M.; Tingoli, M.; Chianelli, D.; Montanucci, M. *Synthesis* **1983**, 751−755.
(13) Broomhead, J. A.; Dwyer, F. P. *Aust. J. Chem.* **1961**, *14*, 250−252.
(14) (a) Gangé, R. R.; Koval, C. A.; Lisenky, G. C. *Inorg. Chem.* **1980**, *19*, 2854−2855. (b) For comparison purposes the potential of the ferrocene−ferrocenium couple was taken as 0.4 V relative to NHE.
(15) Bachman, R. E.; Andretta, D. F. *Inorg. Chem.* **1998**, *37*, 5657−5663.
(16) Blessing, R. H. *Acta Crystallogr.* **1995**, *A51*, 33−38.
(17) (a) *SHELXTL-PC*, version 5.10; Bruker AXS: Madison, WI, 1998. (b) Barbour, L. XSEED, 1999, http://www.lbarbour.com/xseed/.

Table 1. Crystallographic Data for **1**, **2**, **4**, and **5**

	1	**2**	**4**	**5**
empirical formula	$C_{16}H_{12}N_2NiS_2$	$C_{16}H_{12}N_2PdS_2$	$C_{16}H_{12}N_2O_{2.70}PdS_2$	$C_{16}H_{12}N_2O_4PdS_2$
fw, g mol^{-1}	355.11	402.80	446.00	466.80
cryst syst	monoclinic	monoclinic	monoclinic	monoclinic
space group	$P2_1/c$ (No. 14)	$P2_1/c$ (No. 14)	$P2_1/c$ (No. 14)	$P2_1/c$ (No. 14)
temp, K	173	173	193	173
a, Å	7.9920(1)	8.1631(5)	8.026(3)	8.5611(9)
b, Å	1.4385(1)	11.4379(7)	14.600(6)	14.4586(15)
c, Å	16.1415(1)	16.2475(10)	13.371(3)	13.3677(14)
β, deg	103.327(1)	103.7010(10)	101.80(3)	108.122(2)
vol, Å^3	1435.86(2)	1473.84(16)	1533.8(9)	1572.6(3)
density (calcd)	1.643 Mg/m^3	1.815 g/cm^3	1.931 g/cm^3	1.972 g/cm^3
Z	4	4	4	4
abs coeff, mm^{-1}	1.634	1.535	1.498	1.471
reflns collected	15 602	16 579	16 809	17 692
independent reflns	3503 [R(int) = 0.0438]	3561 [R(int) = 0.0276]	3729 [R(int) = 0.0794]	3819 [R(int) = 0.0558]
R indices[a]	R1 = 0.0363 ($I > 2\sigma(I)$) wR2 = 0.0692 (all data)	R1 = 0.0215 ($I > 2\sigma(I)$) wR2 = 0.0495 (all data)	R1 = 0.0611 ($I > 2\sigma(I)$) wR2 = 0.1047 (all data)	R1 = 0.0439 ($I > 2\sigma(I)$) wR2 = 0.1106 (all data)
GOF	1.061	0.950	1.100	0.943

[a] $R1 = \sum||F_o| - |F_c||/\sum|F_o|$; $wR2 = [\sum w|F_o^2 - F_c^2|^2/w(F_o^2)^2]^{1/2}$; GOF (goodness of fit) $= [\sum w|F_o^2 - F_c^2|^2/(n-p)]^{1/2}$; n = number of observed reflections, p = number of parameters.

diffractometer at −100 °C as described elsewhere[15] to provide a complete sphere of data to a resolution of 0.75 Å ($(2\theta_{max} = 56.62°)$: 15 602 reflections (3503 unique, R(int) = 0.0438). Final unit cell parameters were calculated by a least-squares refinement using 8001 reflections culled from the entire data set. The data were corrected for Lorentz and polarization effects, and an absorption correction was applied on the basis of equivalent reflection measurements using Blessing's method as incorporated into the program SADABS.[16] The structure was solved using direct methods and refined against F^2 by full-matrix least-squares methods using the programs incorporated in the SHELXTL/PC suite and XSEED.[17] All non-hydrogen atoms were refined anisotropically, while hydrogen atoms were added in calculated positions using a standard riding model. The final refinement converged with residuals of wR2 = 0.0692 (all data), R1 = 0.0363 ($I > 2\sigma(I)$), and GOF = 1.061. All relevant crystallographic information is included in Table 1, and the significant bond lengths and angles are summarized in Table 2.

2. A dark-red plate approximately 0.38 × 0.16 × 0.14 mm^3 was mounted on a glass fiber using epoxy cement and the data were collected as above, yielding 16 579 reflections (3561 unique, R(int) = 0.0276). Final unit cell parameters were calculated by a least-squares refinement using 4248 reflections culled from the entire data set. The data processing, structure solution, and refinement were carried out as described for **1**. The final refinement converged with residuals of wR2 = 0.0495 (all data), R1 = 0.0215 ($I > 2\sigma(I)$), and GOF = 0.950. All relevant crystallographic information is included in Table 1, and the significant bond lengths and angles are given in Table 2.

4. A pale-yellow plate approximately 0.12 × 0.10 × 0.02 mm^3 was mounted on a glass fiber using epoxy cement and data were collected and processed as above to yield 16 809 reflections (3729 unique, R(int) = 0.0794). Final unit cell parameters were calculated by a least-squares refinement using 6365 reflections culled from the entire data set. During refinement the crystal was found to be a cocrystal of **4** and **5** in a (refined) ratio of 65:35. The length of the second set of S−O bonds, S(1)−O(3) and S(1)−O(4), were loosely restrained to a value of 1.460(5) Å during the final stages of refinement in order to yield a chemically reasonable model. The final refinement converged with residuals of wR2 = 0.1047 (all data), R1 = 0.0611 ($I > 2\sigma(I)$), and GOF = 1.100. All relevant crystallographic information is included in Table 1, and the significant bond lengths and angles are given in Table 2.

5. A pale-yellow block approximately 0.20 × 0.10 × 0.10 mm^3 was mounted on glass fiber using epoxy cement, and data were collected as above to yield 17 692 reflections (3819 unique, R(int) = 0.0558). Final unit cell parameters were calculated by a least-squares refinement using 6988 reflections culled from the entire data set. The final refinement converged with residuals of wR2 = 0.1106 (all data), R1 = 0.0439 ($I > 2\sigma(I)$), and GOF = 0.943. All relevant crystallographic information is included in Table 1, and the significant bond lengths and angles are given in Table 2.

Results and Discussion

Molecular and Electronic Structure. Reaction of $[bpyNiCl_2(dmf)]_2$ and $bdtNa_2$ in a 1:1 mixture of MeOH and CH_2Cl_2 (Scheme 1) led to the immediate precipitation of **1** (Figure 1) as a dark-purple solid. The product was then conveniently isolated and purified by filtration followed by washing with MeOH. The lower solubility of $bpyPdCl_2$ and $bpyPtCl_2$ necessitated the use of DMSO as the reaction solvent. The reaction of $bdtNa_2$ with $bpyPdCl_2$ in DMSO followed by the addition of water gave **2** as a dark-red precipitate (Scheme 1 and Figure 2) in good yield and high purity. Substituting $bpyPtCl_2$ for the palladium complex in this reaction provides **3**, also in good yield and purity.

Our synthetic approaches are similar to those reported previously[2d,9] but offer a few slight advantages. First, by using DMSO rather than DMF as the reaction solvent, we find it unnecessary to employ a silver salt to preactivate the metal center through removal of the halide ligands. Furthermore, use of $bdtNa_2$ in place of $bdtH_2$ eliminates the need for the addition of a base to the reaction mixture. In addition to simplifying the reaction conditions generally, this minor modification makes this synthetic route suitable for a wider range of ligands, particularly those with base-sensitive functions. Moreover, $bdtNa_2$ is significantly more convenient to store and handle than its malodorous and slightly air-sensitive free acid, $bdtH_2$.

Slow evaporation of CH_2Cl_2 solutions of **1** or DMF solutions of **2** in the dark produces deep-purple or red crystals, respectively, of sufficient quality to allow direct confirmation of their structures by X-ray crystallography (Table 1). **1** and **2** are isostructural and isomorphous with each other and their platinum analogue, **3**.[9] Consistent with their isostructural relationship, most of the bond lengths and angles are essentially equivalent for all three complexes (Table 2), with the exception of slightly shorter M−N and M−S bond lengths in the case of **1**. The Ni−N and Ni−S bonds in **1** are slightly shorter than those reported for the related type **C** complex [1,5-bis(2-mercapto-2-methylpropyl)-1,5-diazacyclooctane]nickel(II) [Ni−N = 1.995(3) Å; Ni−S = 2.159(3) Å][18] and slightly longer than those

(18) Darensbourg, M. Y.; Font, I.; Pala, M.; Reibenspies, J. H. *J. Coord. Chem.* **1994**, *32*, 39−49.

Table 2. Selected Bond Lengths (Å) and Angles (deg) for **1**−**5** and Pt(bpy)(bdtO$_4$)

	[(bpy)Ni(bdt)], **1**	[(bpy)Pd(bdt)], **2**	[(bpy)Pt(bdt)], **3**[a]	[(bpy)Pd(bdtO$_2$)], **4**	[(bpy)Pd(bdtO$_4$)], **5**	Pt(bpy)(bdtO$_4$)[a]
M−S	2.144(1)	2.247(1)	2.244(2)	2.230(2)	2.233(1)	2.235(3)
	2.143(1)	2.244(1)	2.250(2)	2.254(2)	2.236(1)	2.218(3)
M−N	1.935(2)	2.067(2)	2.050(4)	2.085(4)	2.109(3)	2.065(8)
	1.939(2)	2.074(2)	2.049(5)	2.096(4)	2.104(3)	2.076(9)
S−O				1.455(4)	1.452(3)	1.462(10)
				1.459(4)	1.462(3)	1.430(9)
					1.463(3)	1.455(8)
					1.457(3)	1.467(9)
C−S	1.756(2)	1.759(2)	1.759(6)	1.781(5)	1.794(4)	1.781(10)
	1.753(3)	1.756(2)	1.762(6)	1.776(6)	1.793(4)	1.780(10)
S−M−S	90.18(3)	88.67(2)	89.0(1)	88.29(5)	87.68(4)	88.9(1)
N−M−N	83.31(8)	79.41(6)	80.1(2)	79.0(2)	78.59(13)	79.3(3)
O−S−O				114.2(3)	114.60(18)	114.3(5)
					114.43(18)	112.4(5)

[a] Taken from Ref 9.

Scheme 1. Synthesis of [M(bpy)(bdt)], M = Ni, Pd, Pt

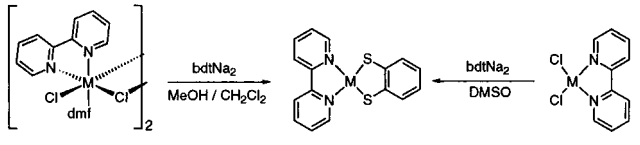

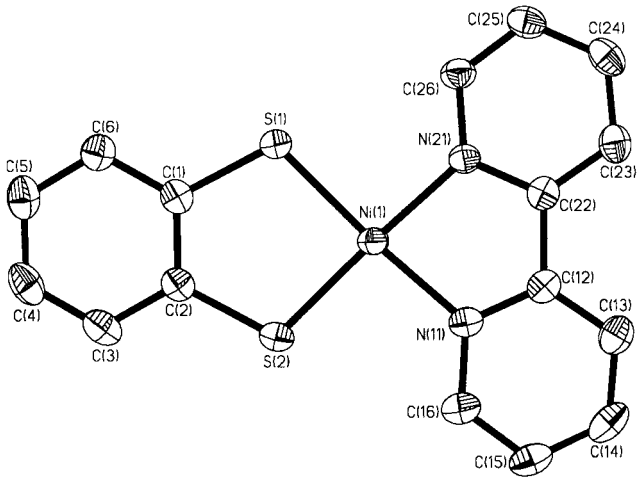

Figure 1. Diagram showing the molecular structure of **1** with the atoms shown with displacement ellipsoids at 50% probability. The hydrogen atoms have been omitted for clarity.

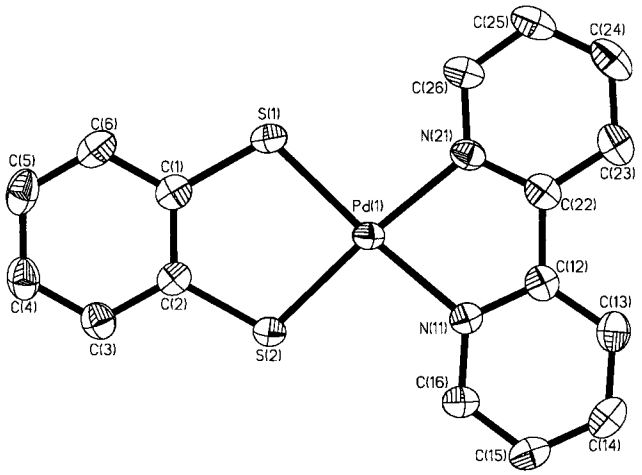

Figure 2. Diagram showing the molecular structure of **2** with the atoms shown with displacement ellipsoids at 50% probability. The hydrogen atoms have been omitted for clarity.

Table 3. UV−Vis and Electrochemical Data[a] for **1**−**3**

	λ_{max} ($CHCl_3$, nm)	ϵ (M^{-1} cm^{-1})	E_{red} (mV)	E_{ox} (mV)
1	557	2500	−1828[b]	84, 634[c]
2	510	2600	−1846[b]	165, 731[c]
3	598	5800	−1775[b]	25, 296[c]

[a] All electrochemical potentials are relative to the Fc/Fc^+ couple. [b] $E_{1/2}$ of reversible process. [c] Peak anodic current of irreversible process.

observed for the type **A** complex [(disn)Ni(tfd)] (disn = diiminosuccinonitrile; tfd = 1,2-trifluoromethylethene-1,2-dithiolate) [Ni−N = 1.861(4), 1.858(4) Å; Ni−S = 2.085(1), 2.089(1) Å].[3c] The Pd−S and Pd−N bond lengths in **2** are essentially equal to those reported for **3**,[9] in keeping with the similar bonding radii of the second- and third-row transition metals.[19] Similar to the trend observed for nickel, the Pd−N and Pd−S bond lengths in **2** are slightly shorter than those observed in the type **C** complex [1,5-bis(mercaptoethyl)-1,5-diazacyclooctane]palladium(II) [Pd−N = 2.093(3) Å; Pd−S = 2.2795(11) Å].[5e] The identity of the metal atom does not seem to have a large structural influence on the dithiolate ligand because the C−S bond lengths are essentially identical in all three cases.

In contrast to their nearly identical solid-state structures **1**−**3** show significant differences in their optical and electronic properties. The most obvious of these differences is the color of the complexes. Crystalline and solution samples of **2** are dark red, whereas both **1** and **3** give deep-purple solids and solutions. Consistent with this qualitative observation, the intense CT absorption that gives rise to the color of these complexes is significantly blue-shifted for **2** (Table 3). Interestingly, this band also appears to be somewhat broadened in the case of **2** (Figure 3). Eisenberg and co-workers have termed this CT process a "mixed-metal-ligand to ligand" transition to highlight that the HOMO involves contributions from the metal atom, the sulfur atoms, and the π system of the aromatic ring while the LUMO is localized on the bipyridine ligand, specifically the π^* orbital.[2f,20] This model implies **1**−**3** share a common LUMO, and hence, any shift in the observed transition energy is principally due to differences in the energy of the respective HOMOs. The latter of these assumptions produces a relative ordering for the energy of the HOMO as a function of metal atom: Pd < Ni < Pt (**2** < **1** < **3**).

(19) Shriver, D. F.; Atkins, P. W. *Inorganic Chemistry*, 3rd ed.; W. H. Freeman and Co.: New York, 1999; pp 23−26.

(20) Zuleta, J. A.; Bevilacqua, J. M.; Proserpio, D. M.; Harvey, P. D.; Eisenberg, R. *Inorg. Chem.* **1992**, *31*, 2396−2404.

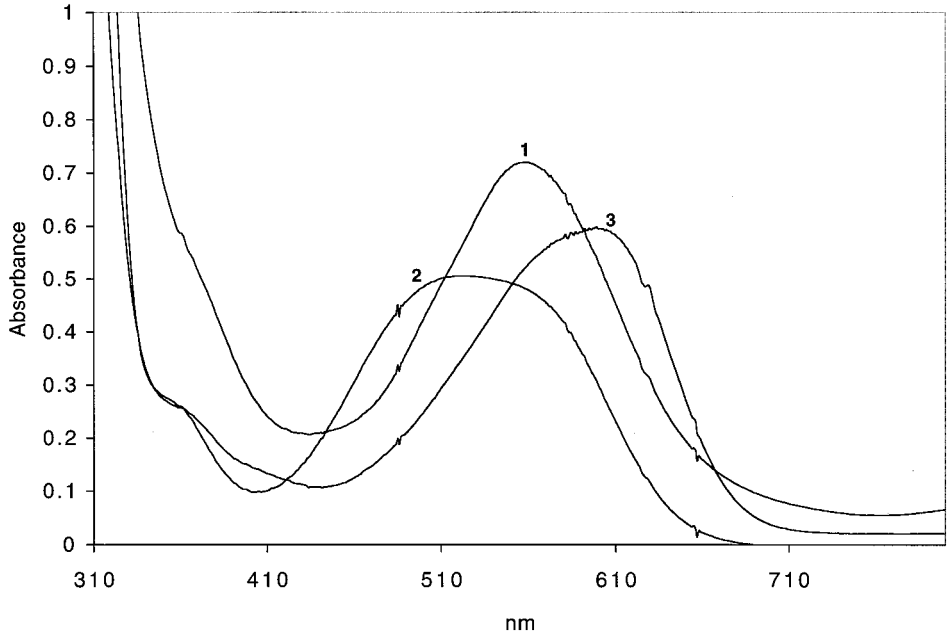

Figure 3. Absorption spectra for **1**−**3**. All spectra were recorded in $CHCl_3$ at concentrations between 1×10^{-4} and 3×10^{-4} M.

To further probe the electronic structure of **1**−**3**, we examined their redox behavior by cyclic voltametry. While CV data for **3** has been reported previously,[9] we chose to reexamine its behavior in order to ensure that all measurements were performed under standard conditions. It should be noted that our results for **3** agree quite well with the previously reported values once the different reference points (NHE vs Fc/Fc^+) are taken into account.[14] All three complexes display a single reversible reduction wave at approximately −1800 mV (Table 3). Since the reduction process can be viewed as the insertion of an electron into the LUMO, this result is consistent with the model presented above in which the LUMO is localized on the π^* orbital of the bipyridine. In contrast to their nearly identical reduction behavior, the three complexes possess significantly different oxidation potentials. While the exact nature of this electrochemical oxidation process remains somewhat unclear,[9] it is reasonable to view the oxidation process formally as the removal of an electron from the HOMO of the complex. Consequently, the first oxidation potential can be used as an alternative measure of the relative HOMO energies. Interestingly, the ordering of orbital energies one arrives at electrochemically is identical to the ordering found spectroscopically, namely, Pd < Ni < Pt. Indeed, there is a strong linear correlation between the optical λ_{max} values (determined in $CHCl_3$) and the first electrochemical oxidation potential (Figure 4). Since the only variable that distinguishes **1**−**3** is the identity of the metal atom, these results strongly support the idea that orbitals on the metal atom make a significant contribution to the HOMO of these systems.

A possible explanation for the somewhat unexpected ordering of the HOMO energies in these complexes (i.e., Pd < Ni < Pt) is the effectiveness of the M(d)−S(p) orbital interactions present. As was noted (vida supra), the M−S bond lengths in the diimine−dithiolene (type **A**) complexes are shorter than those found in related diamine−dithiolate (type **C**) complexes. However, the difference ($d_{(TypeC)} - d_{(TypeA)}$) is twice as large in the palladium case than in the nickel case (0.030 vs 0.015 Å), suggesting a stronger metal−ligand interaction. Unfortunately, we have been unable to find a suitable comparison point for the platinum case in order to test this hypothesis more completely.

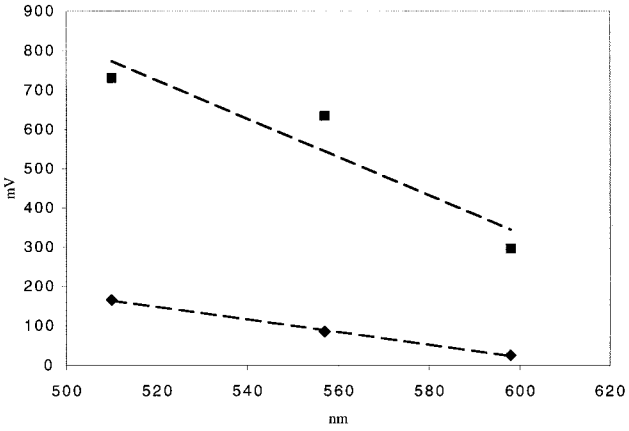

Figure 4. Plot of electrochemical oxidation potentials (mV) vs λ_{max} (nm) for the MMLLCT band. ◆ represents the first oxidation potential, while ■ represents the second oxidation potential. The dashed lines are the linear least-squares fit to the data.

Photochemical and Chemical Oxidation. Connick and Gray recently showed that the photochemical oxidation of **3** produced a mixture of the corresponding monosulfinate (**6**) and disulfinate (**7**) species, with the relative ratio of the two compounds dependent on the choice of solvents and reaction conditions (Scheme 2).[9] In our hands, chemical oxidation of **3** with H_2O_2 yields only **7**, regardless of the reaction stoichiometery.[21] In contrast to these results, we recently showed that the chemical oxidation of **1** leads to an octahedral disulfonate complex (**8**) via rupture of the metal−sulfur bonds and ligand rearrangement.[8] We were also able to isolate an unusual bimetallic complex (**9**) from the slow evaporation of a DMF solution used to determine the electronic spectrum of **1**. In an effort to better understand these widely disparate results, we were interested in unambiguously identifying the oxidation products, both photochemical and chemical, of **2**.

(21) Oxidation of **3** with aqueous H_2O_2 (30%) in DMSO produced a yellow product that was identical by ^1H NMR spectroscopy to the disulfinate complex, $bpyPtbdtO_4$, reported by Connick and Gray (ref 9). ^1H NMR (DMSO, ppm): 9.353 (d, 2H), 8.832 (d, 2H), 8.543 (t, 2H), 8.106 (t, 2H), 7.860 (dd, 2H), 7.727 (dd, 2H).

Scheme 2. Observed Oxidation Pathways for [Ni(bpy)(bdt)] and [Pt(bpy)(bdt)]

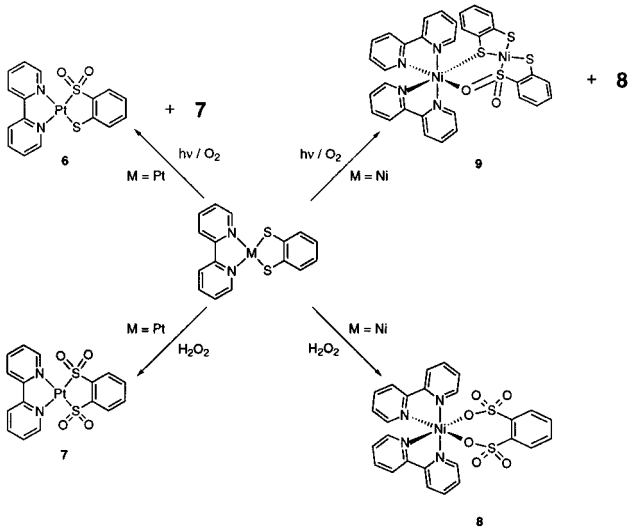

Exposure of an oxygenated DMF solution of **2** to ambient light resulted in a slow color change from dark red to yellow and the formation of pale-yellow crystals as the solvent evaporated over several weeks. Solutions of **2** kept in the dark for a similar length of time showed no apparent color change, demonstrating the role of light in the transformation. X-ray crystallographic analysis of one of these pale-yellow crystals revealed that it was in fact a cocrystal of [Pd(bpy)($bdtO_2$)] (**4**) (Figure 5) and [Pd(bpy)($bdtO_4$)] (**5**). It is significant to note that, as in the platinum case, **4** is always isolated as a mixture with its more highly oxidized cogener, **5**. This would seem to indicate that **4** is, in a sense, a long-lived intermediate in the oxidation pathway leading to **5** that is isolable in large part because the experimental conditions and its relatively low solubility allow it to be sequestered in the solid state before the transformation is complete. Chemical oxidation of **2** with H_2O_2 in DMSO produced an immediate color change of the solution from red to yellow. Again, regardless of the oxidant stoichiometery used, the sole product isolated in this case was the disulfinate complex, **5**. The ^{1}H NMR spectrum of the crude reaction material was consistent with the C_s symmetric nature of the complex and did not indicate any additional bipyridine- or thiolate-containing species. Slow evaporation of a CH_2Cl_2 solution of **5** at room temperature yielded X-ray quality crystals, allowing direct confirmation of the molecular structure of **5** (Figure 6). The essential crystallographic details and important bonding parameters for both **4** and **5** can be found in Tables 1 and 2, respectively.

The structure of **4** was found to be isostructural with **6**,[9] which interestingly was also found to cocrystallize with the closely related disulfinate complex (**7**). Similarly, the only significant structural difference between **5** and **7** was that the latter crystallized as a hydrate. As with the unoxidized complexes, the bonding parameters observed for **4** and **5** and their respective Pt analogues are essentially identical. Additionally, as is the case in the nickel[5] and platinum[9] systems, oxidation of the sulfur atoms does not significantly alter the M−S bond lengths (Table 2). However, oxidation does seem to cause a slight lengthening (ca. 0.024 Å) of the C−S bonds in these complexes. As with the unoxidized complexes, the Pd−N and Pd−S bonds lengths in **4** and **5** are somewhat shorter than those found in the type **C**

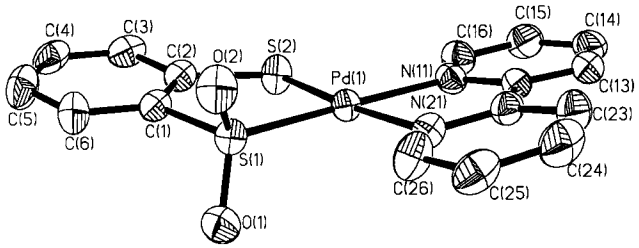

Figure 5. Diagram showing the molecular structure of **4** with the atoms shown with displacement ellipsoids at 50% probability. The hydrogen atoms as well as the oxygen atoms associated with the minor amount of **5** that cocrystallized with this complex have been omitted for clarity.

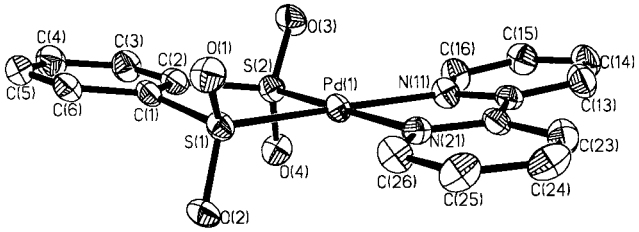

Figure 6. Diagram showing the molecular structure of **5** with the atoms shown with displacement ellipsoids at 50% probability. The hydrogen atoms have been omitted for clarity.

complexes [(tmeda)Pd(II)$(SO_2)_2$R] (R = $-(CH_2)_4-$ or $(CH_3)_2$) [Pd−N(av) = 2.168(4) Å; Pd−S(av) = 2.288(1) Å].[22]

These results, along with those already reported,[8,9] show conclusively that the oxidative reactivity of **2** is identical to its platinum analogue (**3**) while the reactivity of the nickel analogue (**1**) is substantially different. However, as was discussed above, **1** exhibits electronic behavior between that of **2** and **3**. Hence, it seems unreasonable to attribute the difference in reactivity of **1** solely to electronic differences such as frontier orbital energies and/or configurations. Rather, we suspect the observed differences are a consequence of the greater structural flexibility of nickel(II) in relation to its heavier cogeners. Specifically, nickel(II) is known to form complexes readily with higher coordination numbers and geometries, such as octahedral, square pyramidal, and trigonal bipyramidal, while palladium(II) and platinum(II) are found almost exclusively in a square planar geometry. Supporting this hypothesis is the fact that both known sulfonate complexes, **8** and **10**, are octahedral complexes.[7,8]

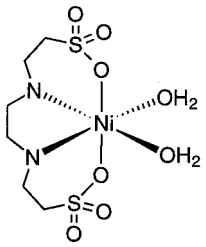

10

Additionally, the O-bound nickel center in **9**, a putative intermediate in the formation of **8**, also possesses an octahedral geometry. Of course the greater affinity of the first-row transition metals for hard ligands such as oxygen also provides a thermodynamic driving force for the formation of O-bound species in the nickel-containing complexes.

(22) Diversi, P.; Ingrosso, G.; Lucherini, A.; Lumini, T.; Marchetti, F.; Merlino, S.; Adovasio, V.; Nardelli, M. *J. Chem. Soc., Dalton Trans.* **1988**, 461−467.

Scheme 3. Proposed "Partial Mechanism" To Rationalize the Formation of **8** and **9**

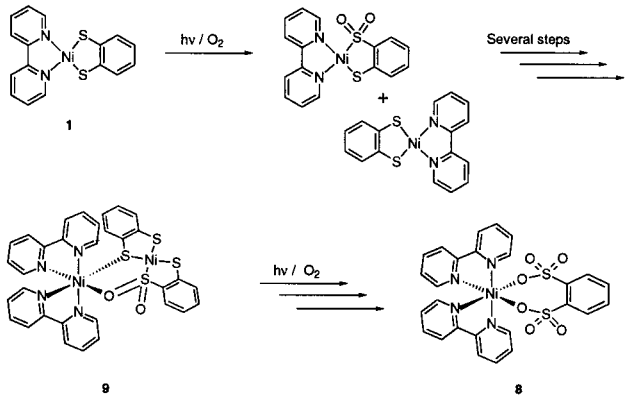

A still open question is the exact mechanistic pathway by which seemingly strong M−S bonds in these complexes are cleaved during their conversion to sulfonate complexes. In the case of **1**, we have previously proposed that **9** is an intermediate in this transformation because it rationalizes both the conversion of the M−S bonds to M−O bonds and the ligand scrambling that is observed (Scheme 3).[8] However, such a binuclear complex seems less likely as an intermediate in the formation of **10** because the nitrogen and sulfur moieties involved are part of a single ligand, ruling out the possibility of an intermolecular ligand transfer as the pathway for converting M−S into M−O bonds. An alternative possibility is that solvent molecules associate with the metal center during this conversion in order to stabilize any intermediates formed during the cleavage of the metal−sulfur bonds. In the case of **10**, two such solvent molecules are incorporated into the coordination sphere of the metal center in the final product. A recent report by Cornman et al. suggests another intriguing possibility.[23] They have characterized a vanadium species with an η^2 S−O bound ligand, which would seem to imply that such a species could be an intermediate in the conversion from S-bound to O-bound ligands in these systems. Of course, the various mechanistic proposals put forth here are not mutually exclusive and more than one may be operative simultaneously.

In conclusion, this work completes the characterization of the principal oxidation products of the type **A** complexes of the nickel triad, specifically those of palladium. Comparison of the optical and electrochemical properties among the series of α-diimine−dithiolene complexes [M(bpy)(bdt)] indicates that the differing oxidative behavior of **1** is unlikely to be the result of differences in the electronic structure of these complexes. Rather, the available evidence seems to indicate that the cleavage of the Ni−S bonds and the subsequent formation of a sulfonate complex are the result of the greater ability of nickel to adopt an octahedral coordination geometry, and perhaps the greater relative thermodynamic stability of metal−oxygen bonds for first-row transition metals. More detailed kinetic and theoretical studies are currently underway to hopefully differentiate between the possible mechanisms for this process.

Acknowledgment. This work was supported by Georgetown University and the Donors of the Petroleum Research Fund, administered by the ACS (No. 31945-G3). Funding for the purchase of the X-ray diffractometer was provided by the National Science Foundation (CHE-9115394) and Georgetown University.

Supporting Information Available: Tables of crystal data, positional parameters, bond distances and angles, and anisotropic displacement parameters for **1**, **2**, **4**, and **5** and an X-ray crystallographic file in CIF format. This material is available free of charge via the Internet at http://pubs.acs.org.

IC000884N

(23) Cornman, C. R.; Stauffer, T. C.; Boyle, P. D. *J. Am. Chem. Soc.* **1997**, *119*, 5986−5987.